Study of Point 4 Chargino Production in an NLC Detector and Observation of Low Energy Biases

Joseph W. Proulx

August 27, 1998

Abstract

This paper describes my attempt to measure the masses of two supersymmetric particles, the chargino and the neutralino. The reaction I studied was $e^+e^- \rightarrow \widetilde{\chi}_1^+\widetilde{\chi}_1^-$, with $\widetilde{\chi}_1^\pm \rightarrow \widetilde{\chi}_1^0 q\bar{q}$. I used the Monte Carlo program ISAJET to simulate data from a linear collider with properties like the proposed Next Linear Collider (NLC), using only those events which produced supersymmertric particles with parameters from the specially derived Point 4 of supersymmetric parameter space. I fit my data to a function that depends on the masses of the chargino and the neutralino, and analyzed sources of low energy biases. This analysis showed that the current design for the NLC detector is limitting for this point.

Contents

List of Tables

List of Figures

1 Introduction

1.1 The Standard Model

The Standard Model (STMD) describes the particles that make up the universe and the interactions among them. It has been extremely succesful in modeling the interactions between elementary particles, and has become the most basic theory for describing the everyday world.

There are two classes of particles, the fermions and the bosons, which are distinguished by their spin quantum numbers. This is a unitless quantity which all particles posess, related to angular momentum. Fermions have half integer spin quantum number, while bosons have integer spin quantum number.

The fundamental fermions are further split into two classes, the leptons and the quarks, each of which contain three families composed of two particles and two antiparticles, as shown in Table 1. An antiparticle is the charge conjugate of another particle. This means it has opposite charge, lepton, and baryon quantum numbers. The leptons consist of the electron, the muon, and the tau, massive particles with charge ∓1; and the electron, muon, and tau neutrinos, light chargeless particles. The quarks consist of the up, charm, and top quarks, with charge $\pm2/3$; and the down, strange, and bottom quarks, similar to the up, charm, and top, but with charge $\mp1/3$.

Table 1: The Fundamental Fermions

	leptons		quarks	
charge	∓1	0	$\pm2/3$	$\mp1/3$
particle	e	ν_e	u	d
	μ	ν_μ	c	s
	τ	ν_τ	t	b

The fundamental bosons regulate the interactions between particles. Their properties are listed in Table 2. In addition, the graviton, a massless, spin 2 particle that has never been observed, regulates gravitational interactions. However, particle physics currently has no satisfactory model of gravity. The rest of the fundamental bosons have spin 1. The photon, also massless, regulates the electromagnetic interaction, which affects all charged particles. The W^+, W^-, and Z^0 are massive and regulate the weak interaction, which relates to particle decays. The massless gluon regulates the strong force, which affects all quarks and the gluon itself. The strong force has such a great effect that no quarks have ever been observed alone, but instead are always bound to other quarks to form hadrons, such as the proton (uud) and π^- ($\bar{u}d$).

Table 2: The Fundamental Bosons

boson	graviton	photon	$W^{\pm}$, Z^0	gluon
spin	2	1	1	1
mass	0	0	80.33, 90.19	0
interaction	gravity	electro-magnetic	weak	strong

Interactions occur when a particle emits or absorbs another, or when particles decay. Some of their properties are listed in Table 3 These interactions all follow certain conservation laws, including the conservation of energy, momentum, charge, and lepton number. The conservation laws describe which processes may occur. The probability of each process depends on dimensionless coupling constants of the four forces. For example, the gravitational coupling constant is so small, 4.6×10^{-46}, that gravitational interactions are negligible at atomic scales, which is why the graviton has never been observed in particle colliders. The electromagnetic coupling constant is about 1/137, making electromagnetic interactions much more common.

One serious flaw exists in the STMD. On its own, it describes a world of massless particles. To obtain mass, particles couple to a field called the Higgs field. However, these couplings also cause infinite corrections to the

Table 3: The Fundamental Interactions

force	gravity	electro-magnetic	weak	strong
carrier	graviton	photon	$W^{\pm}$, Z^0	gluon
source	mass	charge	isospin	color
acts on	all massive particles	all charged particles	fundametal fermions, weak gauge bosons	quarks, gluons

mass of the associated Higgs particle. New physics is required to explain how to obtain a finite Higgs mass. For this reason, physicist are searching for new models to augment the STMD.

1.2 Supersymmetry

Supersymmetry (SUSY) is an important hypothesis that goes beyond the STMD. It describes a new set of particles, called sparticles, that parallel the known particles, but each of which has spin quantum number that differs by 1/2 from its STMD partner. Thus, SUSY describes a symmetry between fermions and bosons. The symmetry is not perfect: the sparticles are expected to have much higher mass than STMD particles since none have been detected yet.

An important motivation for SUSY is that it makes it possible to calculate the mass of the Higgs particle, which physicists expect to discover soon. Because SUSY introduces new particles, it also introduces new corrections to the Higgs mass. These new corrections are expected to completely cancel the corrections of the STMD, allowing a finite Higgs mass. A related effect is that SUSY requires five Higgs particles instead of just one.

A second motivation for SUSY stems from the search for a Grand Unification Theory (GUT), which would attempt to explain the electromagnetic, weak, and strong forces as aspects of a single force. To do this, the three coupling constants of the forces, α_{em}, α_w, and α_s, must converge to one value at some extremely high energy. Even at the relatively low energies currently used, the coupling constants change. For example, α_{em} is 1/137 at very low energies, but increases to about 1/128 for energies near the Z^0 center of mass energy. This is because there is more opportunity for intermediate virtual processes, which change the coupling constants, to occur at higher energies. With only the STMD, theorists predict that the three coupling constants do not converge at one point; the energy at which α_{em} and α_w converge is lower than the energy at which either converges with α_s. Introducing SUSY into this calculation makes the points of convergence much closer together.

For these reasons, SUSY is an important part of the solution to long-standing problems, and a search for sparticles is necessary. SUSY also introduces a pleasing symmetry into nature, making it one of the most interesting and important hypotheses in high energy physics today.

2 SUSY at the NLC

One of the possible manifestations of SUSY is the mSUGRA (minimal supergravity-inspired) model, which could include the postulate of R-parity (R_p) conservation. The quantity R_p is given by,

$$R_p = (-1)^{3B+L+2S} \tag{1}$$

where B is the baryon number, 1/3 for quarks; L is the lepton number, ± 1 for leptons; and S is the spin. For STMD particles, R_p is 1, while for sparticles R_p is -1. Many theorists expect that R-parity is conserved; that is, that the product of the R_p values for all particles at each vertex in a Feynman diagram is 1. This means that there must always be an even number of sparticles at a vertex. Thus, each sparticle decays into another sparticle and any number of STMD particles.

The lightest supersymmetric particle (LSP) can never decay. It is expected that the LSP will be neutral, the supersymmetric partner to a neutrino or a chargeless guage boson, and will thus always escape detection, making it much more difficult to measure the properties of sparticles. Since sparticles are very massive, they will carry away a large amount of energy if R-parity is conserved. This energy loss is the hallmark of SUSY.

If R-parity is violated, allowing all decay products to be seen, SUSY could be detected in the near future at the Large Hadron Collider (LHC), a proton - antiproton collider at CERN in Switzerland. Since protons are hadrons, made up of three quarks, the collisions are much more complicated than the collisions at an electron - positron collider like the NLC will be. Thus the NLC will play an important role in measuring masses, cross sections, and branching ratios, and will cover all aspects of SUSY phenomenology.

The NLC will produce highly focused beams of electrons and positrons at energies starting at 250 GeV, producing 500 GeV of available energy when two particles collide. It will have a detector with a very strong, 4 Tesla magnet, which will allow precise momentum measurements for charged particles. It will also have very good calorimetry for electrons and photons, and it will be able to identify muons with great accuracy. However, the hadronic calorimetry will be somewhat worse than the electromagnetic calorimetry. The NLC will also be able to strongly polarize the spin of the electron beam, and perhaps even polarize the positron beam as well. This is important because sparticle production depends strongly upon the amount of longitudinal polarization of the electron and positron that produce it.

3 Generation of Events

3.1 SUSY Parameter Space

Since SUSY has not been tested, it may work in a number of ways. Theorists have considered several possible models, including the mSUGRA model, described by a certain set of parameters. While any point in this parameter space may describe the correct model of SUSY, theorists have chosen five points to represent possible scenarios. The sparticles described by these points are shown in Table 4. For each, the LSP is the neutralino[1] ($\widetilde{\chi}_1^0$). Experimentalists hope that if they can design a detector that will work well for all of these points, then it will probably work well to study SUSY in the form that exists in nature.

[1] In this paper, *neutralino* will refer to the $\widetilde{\chi}_1^0$, not the $\widetilde{\chi}_2^0$, $\widetilde{\chi}_3^0$, or $\widetilde{\chi}_4^0$, unless otherwise specified; similarly, *chargino* will refer to the $\widetilde{\chi}_1^{\pm}$, not the $\widetilde{\chi}_2^{\pm}$.

Table 4: Mass Spectrum for the Five SUSY Points [3]

	Point 1	Point 2	Point 3	Point 4	Point 5
$\widetilde{\chi}_1^0$	86.05	128.70	44.52	77.83	57.17
$\widetilde{\chi}_2^0$	175.45	257.22	97.00	115.29	111.46
$\widetilde{\chi}_3^0$	492.70	535.50	256.94	146.84	444.77
$\widetilde{\chi}_4^0$	501.75	542.54	273.64	292.41	464.60
$\widetilde{\chi}_1^\pm$	175.34	257.20	96.39	96.06	110.10
$\widetilde{\chi}_2^\pm$	500.81	542.24	272.04	292.46	461.60
h^0	83.25	89.92	68.29	126.96	101.42
H^0	745.30	681.40	378.99	201.61	622.61
A^0	741.05	676.41	371.09	200.00	620.01
$H^\pm$	744.61	680.33	378.49	214.81	624.10
$\widetilde{\nu}_\ell$	421.40	230.02	206.62	1000.00	314.60
$\widetilde{e}_L^\pm$	425.92	238.21	215.70	1000.00	320.64
$\widetilde{e}_R^\pm$	408.80	156.95	206.54	1000.00	307.45
$\widetilde{t}_1$	424.43	535.82	263.71	924.84	150.66
$\widetilde{b}_L$	520.57	621.86	274.27	1000.00	380.76
$\widetilde{q}_{L,R}$	603.27	668.31	316.73	1000.00	462.49
$\widetilde{t}_2$	550.61	656.48	329.48	1096.29	494.73
$\widetilde{b}_R$	595.55	653.10	312.97	1000.00	456.58
$\widetilde{g}$	550.62	759.04	298.40	900.00	425.25

3.2 Monte Carlos and Analysis Programs

I chose Point 4[2] to study. This point has low mass charginos and neutralinos, and charginos dominate the SUSY production modes. To generate events, I used *ISAJET*, a Monte Carlo program that has worked well in the past to model hadron decays. I had it simulate 10^7 seconds, or one running year, of SUSY events. This represents an integrated luminosity of 50 fb^{-1} for the present NLC design. I used an energy of 500 GeV, and an electron left-handed polarization of 60 percent.

[2]While Points 1, 2, 3, and 5 come from mSUGRA parameter space, Point 4 has a slightly different set of parameters, and is not truly an mSUGRA point.

I then processed the events using a program called *NLCPROC* [3] which calculated important quantities associated with the events and individual particles, and which smeared the 4-vector values of all visible particles to account for resolution and inefficiencies in the NLC detector. *NLCPROC* converted the data into ntuples in a form that CERN's Physics Analysis Workshop (*PAW*) could use. I used *PAW* to do all of my analysis.

3.3 Point 4 Production and Decay Modes

At this energy and polarization, the most prominent production mode is $e^+e^- \to \widetilde{\chi}_1^+\widetilde{\chi}_1^-$. Feynman diagrams for this reaction are shown in Figure 1. Point 4 charginos have two important decays. Most of the time, the decay is $\widetilde{\chi}_1^\pm \to \widetilde{\chi}_1^0 q\bar{q}$, but one one third of the time, it is $\widetilde{\chi}_1^\pm \to \widetilde{\chi}_1^0 \ell\nu_\ell$. The only other important SUSY production modes are $\widetilde{\chi}_1^0\widetilde{\chi}_2^0$ and h^0Z^0. The cross sections for these modes are listed in Table 5; some important decay modes are listed in Table 6.

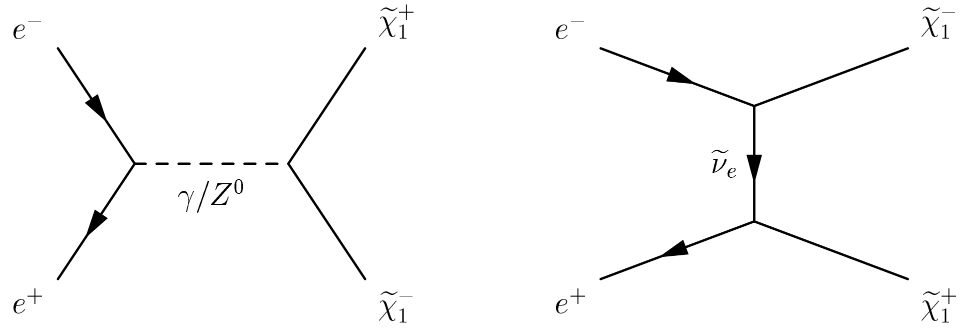

Figure 1: Two Feynman Diagrams for Chargino Production. Right is the SUSY analog to W^+W^- production via neutrino exchange.

Table 5: Various Point 4 NLC Production Modes and Cross Sections at 500 GeV, 60% Right Polarization [3]

Production Mode	Cross Section (fb)	Production Mode	Cross Section (fb)
$\widetilde{\chi}_1^+\widetilde{\chi}_1^-$	697	$\widetilde{\chi}_2^0\widetilde{\chi}_3^0$	26
$\widetilde{\chi}_2^+\widetilde{\chi}_2^-$	8	$h^0 Z^0$	64
$\widetilde{\chi}_1^0\widetilde{\chi}_1^0$	6	$H^0 A^0$	12
$\widetilde{\chi}_2^0\widetilde{\chi}_2^0$	1	$H^+ H^-$	22
$\widetilde{\chi}_1^0\widetilde{\chi}_2^0$	175		

Table 6: Various Point 4 Branching Ratios [3]

Particle	Branching Ratios mode	fraction(%)
$\widetilde{\chi}_1^+$		
	$\widetilde{\chi}_1^0 q\bar{q}$	66.7
	$\widetilde{\chi}_1^0 e^+\nu_e$	11.1
	$\widetilde{\chi}_1^0 \mu^+\nu_\mu$	11.1
	$\widetilde{\chi}_1^0 \tau^+\nu_\tau$	11.1
$\widetilde{\chi}_2^0$		
	$\widetilde{\chi}_1^0 q\bar{q}$	68.8
	$\widetilde{\chi}_1^0 \ell^+\ell^-$	9.1
	$\widetilde{\chi}_1^0 \nu\bar{\nu}$	18.1
	$\widetilde{\chi}_1^\pm \ell^\mp\nu_\ell$	4.0
h^0		
	$q\bar{q}$	88.0
	$\tau^+\tau^-$	5.3
	$W^\pm q\bar{q}$	3.4
Z^0		
	$\ell^+\ell^-$	10.1
	$\nu\bar{\nu}$	20.0
	$q\bar{q}$	69.9

Since the $\widetilde{\chi}_1^0$ is invisible, the visible products of the $\widetilde{\chi}_1^0\widetilde{\chi}_2^0$ mode all come from the $\widetilde{\chi}_2^0$. Most of these decays produce a $\widetilde{\chi}_1^0$ and quark jets. A few produce a chargino, lepton, and neutrino. The $h^0 Z^0$ mode has a more distinctive signature. Usually, all decays are visible, producing an event more typical of Standard Model events[3]. Sometimes, when the Z^0 decays into neutrinos and is thus invisible, it behaves like a $\widetilde{\chi}_1^0\widetilde{\chi}_2^0$ events where the $\widetilde{\chi}_2^0$ produces quarks. The Higgs almost always decays into hadrons.

4 Cuts

In order to isolate my signal from the SUSY background and to ensure that I could analyze it acurately, I employ three cuts on the data. These cuts remove enough background that about 95 percent of the remaining data comes from my signal, with the remaining background causing no significant biases. The cuts also retain enough data to allow analysis. The visible energy spectra for the signal and for all SUSY data before these cuts are shown in Figure 2.

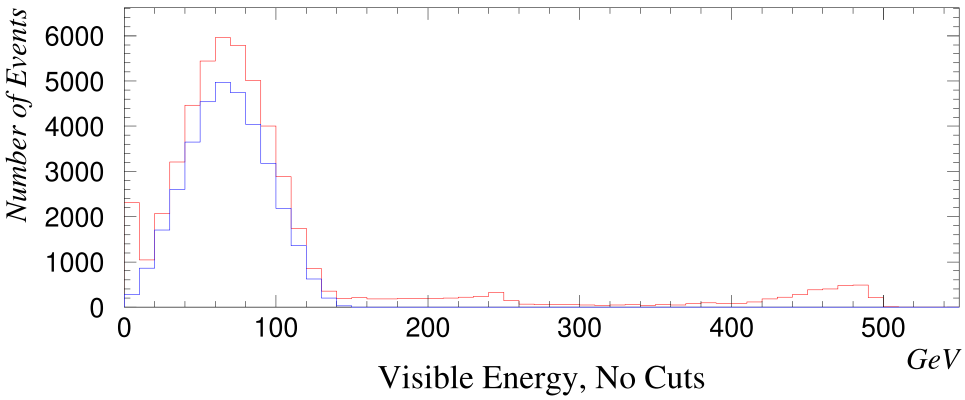

Figure 2: Red - All SUSY Data, Blue - Signal. The signal is quite strong, and accounts for the majority of the SUSY events.

[3]The Higgs particles have R_p of 1, as described by equation 1, and are thus, strictly speaking, Standard Model particles. However, their masses are important variables in mSUGRA SUSY, and are being incorporated into this simulation for that reason

4.1 Cut 1

The first cut looks for events where exactly one of the jets produced contains one lepton and no other particles. A jet is a group of detected particles moving in approximately the same direction, indicating that they may have been produced as the result of the hadronization of a given quark. Events with solitary leptons occur when one of the initial charginos decays into a neutralino and a virtual $W^{\pm}$ particle, which immediately decays into a muon or electron and its associated neutrino. An identical situation occurs when the $W^{\pm}$ decays into a tau, which then decays into an electron or muon. Feynman diagrams for these decays are shown in Figure 3. This process simply produces two extra tau neutrinos. Since the neutralino is the LSP, this means that the only visible particle produced by the chargino is the lepton. This lepton is unlikely to go in the same direction as any other particle, so the jet finding routine in *NLCPROC* declares it an isolated jet, made up of one particle.

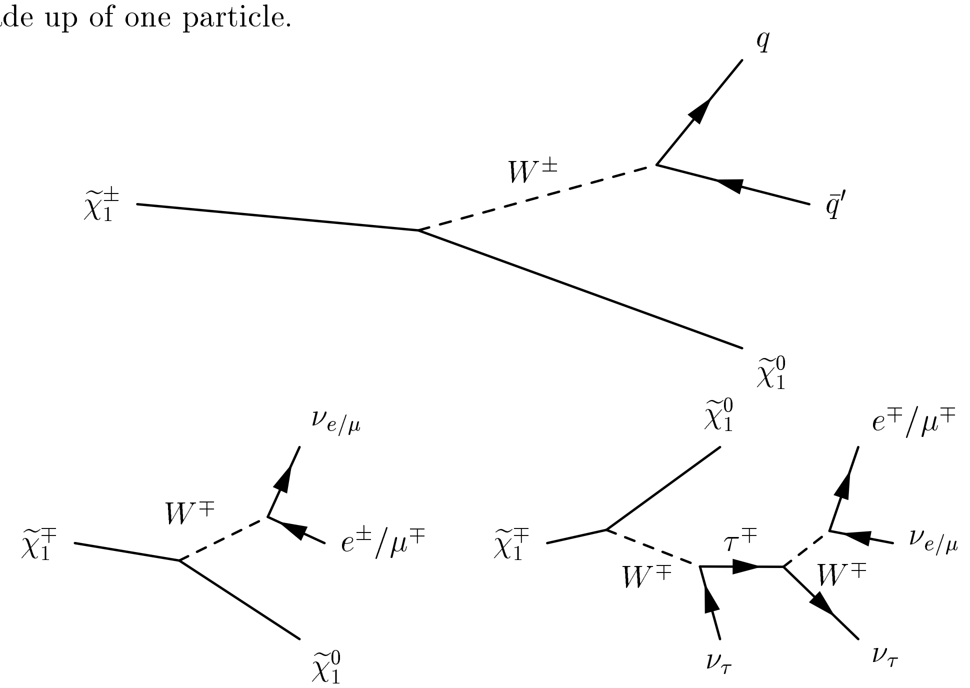

Figure 3: Three Feynman diagrams for important chargino decays. Always, one neutralino is produced immediately, along with a virtual W. Above, the W produces quarks, which hadronize. Below, the W produces leptons and neutrinos. Occasionally, this happens via a tau.

However, since this process has too many invisible particles to be useful for measuring the mass of the sparticles, I required that the other chargino does not produce a solitary lepton. Instead, the virtual W in this case must decay into a $q\bar{q}$ pair, which hadronizes into mostly visible particles. This process is also shown in Figure 3. The result is to completely separate the decay products of each chargino, and retain enough information to do analysis. This also proved to be the most important cut for reducing background.

4.2 Cut 2

The next cut removes all events producing any extra electrons or muons. These events occur when hadron decays produce lepton-neutrino pairs, a process known as semi-leptonic decay. This can skew the data, as energy and momentum are lost to the neutrino. Thus, this cut is not intended to remove not any specific background; rather, its purpose is to remove signal events that cannot be analyzed correctly.

4.3 Cut 3

The final cut is also intended to remove troublesome signal events. For this cut I compute the combined mass of all the visible particles except the lepton from the first cut. This calculation assumes that all the particles come from one initial particle, and then computes the mass of that particle using relativistic kinematics. Since energy and momentum are always conserved, the sums of the energy and momentum of these particles equals the energy and momentum of the original particle. After taking these sums, the mass is calculated from the relation,

$$E^2 = P^2 + M^2. \tag{2}$$

This cut requires that the combined mass be greater than the tau mass. This is because taus often decay into two quarks and a tau netrino. Thus, a chargino decay producing a tau which then decays into a neutrino and a $q\bar{q}$ pair would be accepted by the first two cuts whenever the other chargino produced a visible lepton. Luckily, all the visible particles in this event, excepting the lepton from the first cut, come from the tau. Therefore, the combined mass will certainly be no greater than the tau mass. Thus, this cut further cleans up my signal.

4.4 Results

The result of the three cuts eliminate nearly all of the background, as shown in Table 7 and Figure 4. The first cut dramatically increases the ratio of the number of accepted signal events to the number of all accepted events (the signal to data ratio). It also reduces the number of events in the signal by almost two thirds. The chargino branching ratio indicates that this cut should remove five ninths of the signal. The other events removed by the first cut include those producing semi-leptonic decays whose visible lepton is declared an isolated jet. The second and third cuts do very little to change either the signal acceptance or the signal to data ratio.

The plots of signal and background for the quantities important to this study also show that the background is negligible, as shown in Figure 5. These quantities are jet energy and the combined mass of the jets. Jet energy is simply the energy of the particles produced by the initial virtual W, calculated by summing the energy of all particles except the solitary lepton. The combined mass is calculated with the same particles, using equation 2.

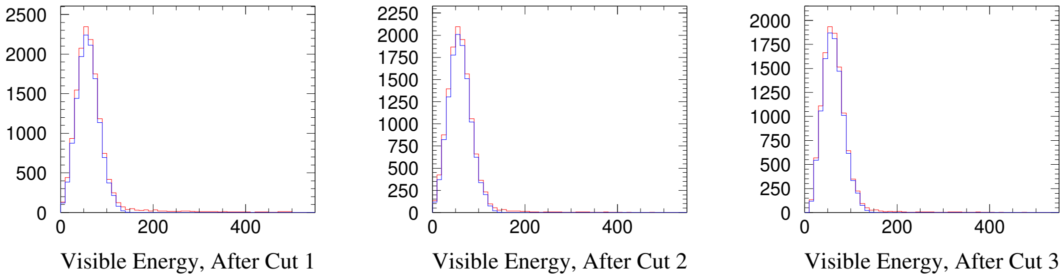

Figure 4: Red - All SUSY Data, Blue - Signal. Cut 1 removes nearly all of the background, as well as two thirds of the signal. Cuts 2 and 3 have minor effects on the signal to data ratio and the signal acceptance.

Table 7: Result of Cuts 1,2,3

Cut	Events		Signal to Data	Signal
	All Data	Signal	Ratio	Acceptance
None	51250	34959	68%	100%
1	14730	13348	91%	38%
2	13003	12075	93%	35%
3	11390	10733	94%	31%

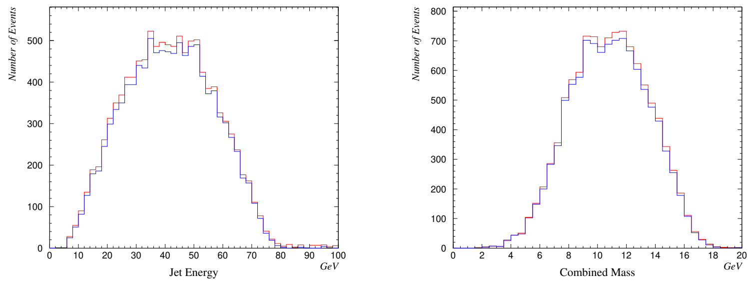

Figure 5: Jet energy, left, and combined mass, right, for data remaining after Cuts 1, 2, and 3. Red - All SUSY Data, Blue - Signal.

5 Mass Computations

5.1 Methods

5.1.1 The Endpoint Method

In the case of a two body decay, $A \rightarrow B + C$, the energy of each decay product varies over a flat distribution. The masses of the particles and the initial energy of particle A uniquely determine the distribution's endpoints. Thus, after many events, one can calculate the mass of the initial particle, A, and one decay product, B, given the mass of the observed particle, C, by measuring particle C's energy distribution. The masses are calculated using the following relations [1, 2, 4]:

$$M_A^2 = \frac{(M_C^2 + E_{C,max}E_{C,min}) \pm \sqrt{(M_C^2 - E_{C,max}^2)(M_C^2 - E_{C,max}^2)}}{(E_{C,max} + E_{C,min})/2E_A^2} \tag{3}$$

$$M_B^2 = M_A^2 + M_C^2 - M_A^2 \frac{E_{C,max} + E_C, min}{E_A} \tag{4}$$

In the case of Point 4 charginos, the visible decay product is the virtual W. Because it is virtual, it has no definite mass. Thus, this method must be refined to allow a variable M_C. One can modify it in two ways to account for the distribution of combined mass.

5.1.2 A Modified Endpoint Method

The simplest modification is to recombine the W mass and make cuts accepting only a small range of mass, say from 10 GeV to 12 GeV, and then use the resulting energy distribution to make an energy calculation. This method has two problems. First, it may cut so many events that there are not enough left to make a good measurement. Second, the endpoints may change between 10 and 12 GeV. This would mean that regardless of the number of events, there could be no sharp endpoint. The one advantage is

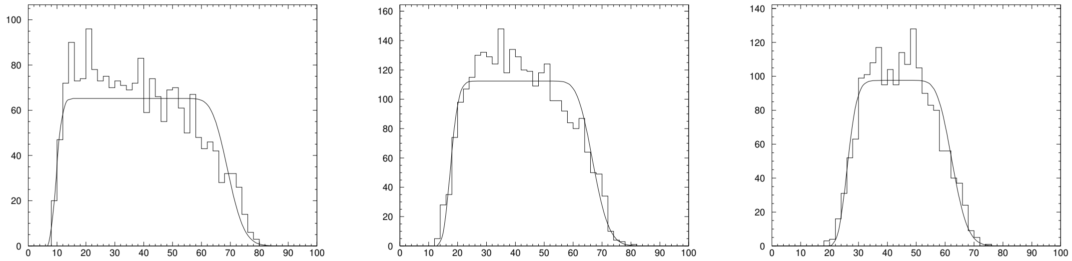

Figure 6: Jet Energy (total visible energy minus isolated lepton energy) for $W^{\pm}$ between 7 and GeV (left), 10 and 12 GeV (middle), and 13 and 15 GeV (right). The fit allows for energy resolution in the hadronic calorimeter, by convoluting the box function with a gaussian with $\sigma = 0.1e + 0.45\sqrt{e}$, smoothing out the discontinuities in the box function.

Table 8: Results of Modified Endpoint Method

		$\widetilde{\chi}_1^{\pm}$ (96.06 GeV)		$\widetilde{\chi}_1^0$ (77.83 GeV)	
Mass Range	χ^2 for fit	Mass (GeV)	Discrepancy	Mass (GeV)	Discrepancy
8 ± 1 GeV	2.7	84.3	-12%	70.2	-9.8%
11 ± 1 GeV	2.6	82.7	-14%	68.1	-13%
14 ± 1 GeV	2.2	87.6	-8.8%	71.7	-7.9%
Average		84.9	-11%	70.0	-10%

that it is possible to take several selections; for example the intervals from 7 to 9 Gev, from 10 to 12 GeV, and from 13 to 15 GeV. Energy distributions for these intervals are shown in Figure 6, while the corresponding calculations are given in Table 8. In no case was the fit very good, and the discrepancies were quite large.

5.1.3 A Two-Dimensional Fit

Instead, I used a fit not only to energy, but also to mass. The combined mass of the virtual W's seemed to fall in a normal distribution, as seen in Figure 8. A gaussian fit showed that this was a very good approximation.

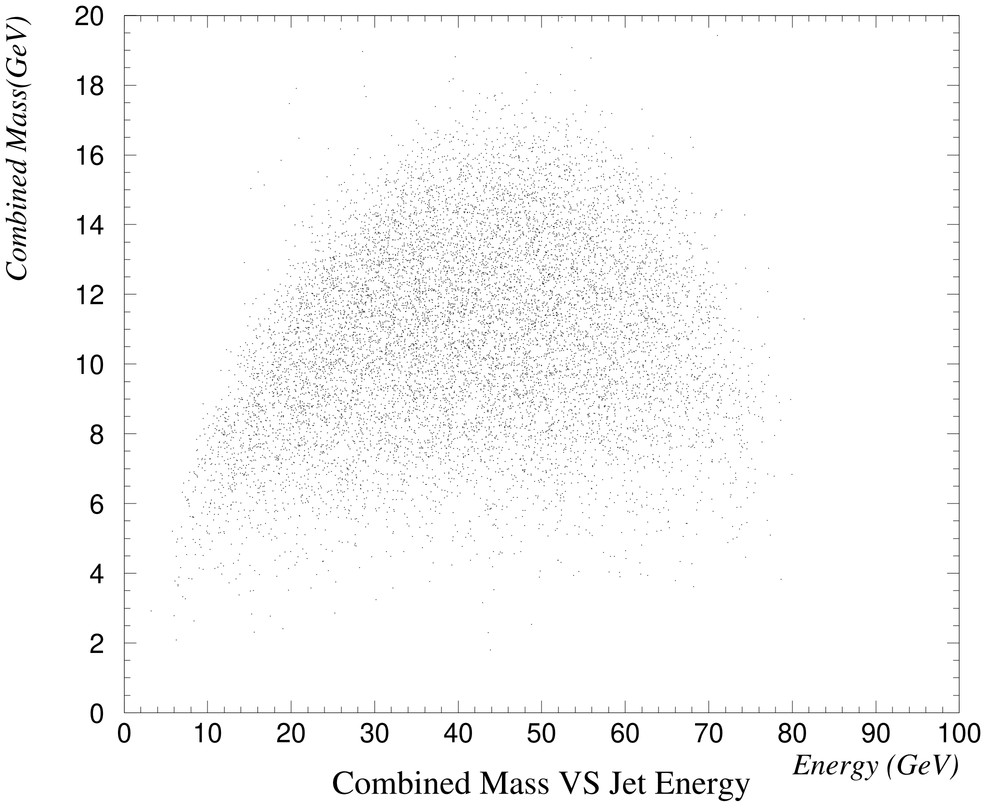

Figure 7: Energy VS Combined Mass of the virtual W particle produced by the chargino. The minimum and maximum possible energies depend upon the combined mass of the virtual W.

For each value of mass, there should be a be a flat distribution of energy. Thus, plotting mass against energy, the resulting probability distribution of points in the energy-mass plane should depend solely on the two unknown masses. This plot appears in Figure 7. Fitting a surface to the data should immediately yield measurements of these masses.

The appropriate surface is given as follows, as a function of $M_{\widetilde{\chi}_1^\pm}$ and $M_{\widetilde{\chi}_1^0}$. First, let h be the height of the surface. This gives

$$h(E, M) = k \cdot p[M] \cdot p[E|M]$$

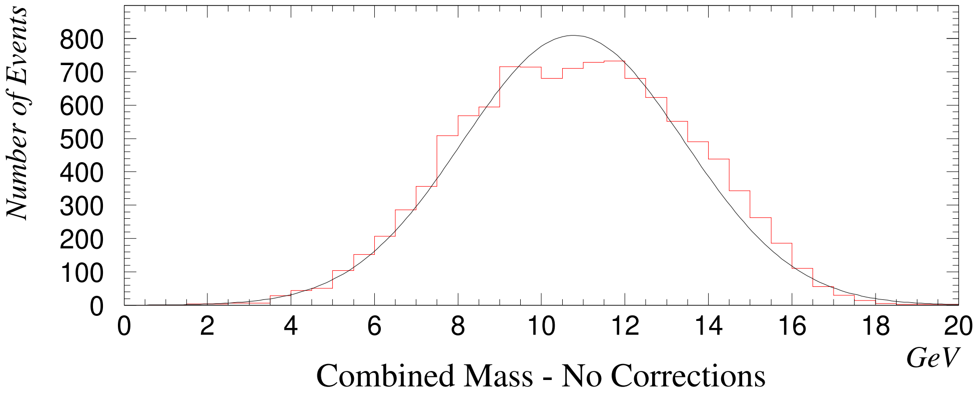

Figure 8: Gaussian fit for $W^{\pm}$ combined mass

where $p[M]$ is the probability of the combined mass falling into the bin range associated with the mass M, and $p[E|M]$ is the probability of the energy falling into the bin range associated with the energy E. Note that $p[E|M]$ depends on the combined mass, as the combined mass affects the endpoints of the distribution. The variable k can be considered a normalization factor.

Next, $p[M]$ is a simple gaussian distribution. Since there is a normalization constant in the function already, there is no need to normalize this distribution.

$$p[M] = e^{\frac{(M-\mu)^2}{2\sigma^2}}$$

Finaly, $p[E|M]$ is a flat distribution. In this case it is necessary to normalize so that each mass M gives $\int p[E|M] = 1$. With this condition, $p[E|M]$ is given by

$$p[E|M] = \begin{cases} \frac{1}{E_{max}-E_{min}} & E_{min} < E \text{ and } E < E_{max}, \\ 0 & \text{otherwise,} \end{cases}$$

where E_{min} and E_{max} are the endpoints of the energy distribution, given by equations 3 and 4. Thus, the mass dependence appears only in the width of the surface at a given mass. Note that the above is a simplification; the value of $p[E|M]$ that I used was the above box function convoluted with the appropriate gaussian distribution.

Finally, combining these yields

$$h(E,M) = k \cdot e^{\frac{(M-\mu)^2}{2\sigma^2}} \cdot p[E|M](M_{\widetilde{\chi}_1^\pm}, M_{\widetilde{\chi}_1^0}), \tag{5}$$

which has three variables, k, $M_{\widetilde{\chi}_1^\pm}$, and $M_{\widetilde{\chi}_1^0}$. Thus, the PAW function fitting routine tests masses directly for agreeement with the data, rather than testing some variable that depends on the masses.

The immediate benefit of this method is that it uses all the data to make a calculation. While the previous method allows many computations, it is diffcult to determine which are the most reliable. This method intrinsically weights the importance of each combined mass. However, it requires many more bins than a 1 dimensional fit, increasing the statistical fluctuations. This is not a large disadvantage over the previous method because while it decreases the bin size, it uses all the entries. Another benefit is that the maximum combined mass of the fit corresponds to the difference in the masses of the $\widetilde{\chi}_1^\pm$ and the $\widetilde{\chi}_1^0$. Overall, this was the better method.

5.2 Results

I used this method to do the mass calculations. This produced figures for the mass of the chargino and the neutralino that were too low, as shown in Table 9. However, while the χ^2 for the fit was rather high, a plot of the data seemed to agree with the plot of the fit. The positions of the boundaries, in particular, seemed to agree quite well, as shown in Figure 9. Since the boundary is what determines the masses, I felt that the large χ^2 was not causing the discrepancy.

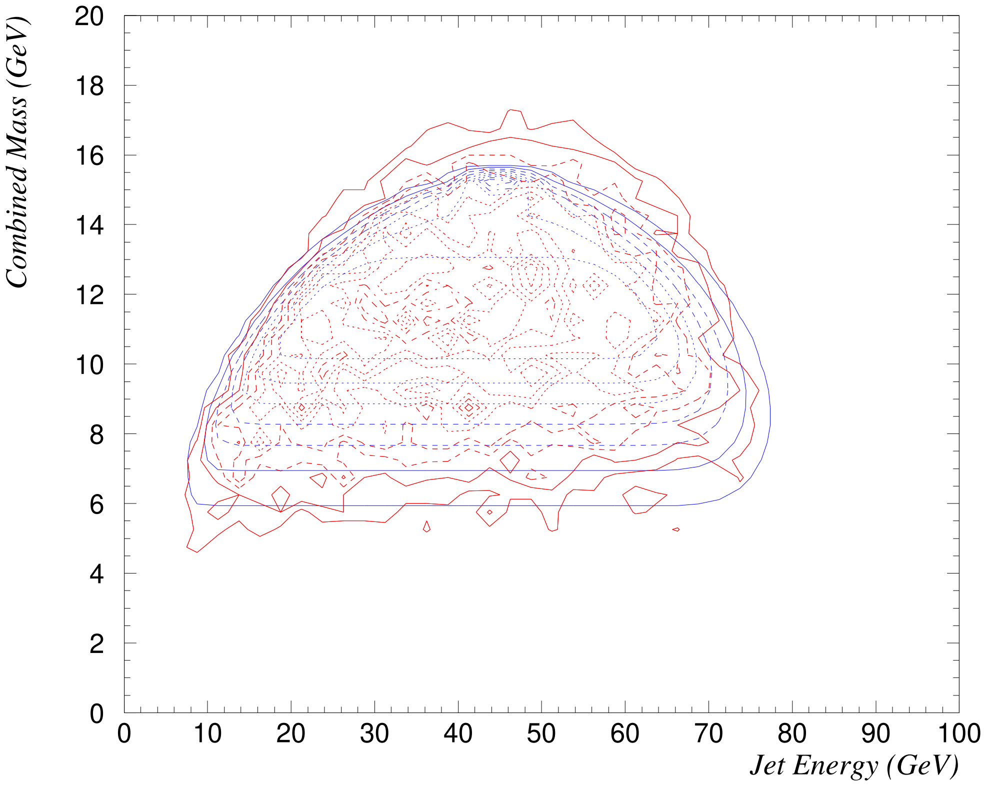

Figure 9: Red - Data, Blue - Fit. While there is some discrepancy between the height of the bins and the fit, the edges, most significant for the mass calculations, correspond well for most values. The maximum combined mass, given by $M_{\tilde{\chi}_1^\pm} - M_{\tilde{\chi}_1^0}$, is too small in the fit.

Table 9: Results of 2-Dimensional Fit

parameter	input value	fit value	approximate error in fit	discrepancy	χ^2/d.o.f.
$M_{\tilde{\chi}_1^\pm}$ (GeV)	96.06	87.8	± 0.2	-8.6%	2.5
$M_{\tilde{\chi}_1^0}$ (GeV)	77.83	72.4	± 0.2	-7.0%	
height	(none)	938	± 8	(none)	

6 Sources of Bias

I checked several sources of bias. The main problem was that the W mass distribution is different than it should be. While the maximum combined mass should be 18.23 GeV, the fit stops at about 16 GeV. I used 4-vector values that were stored without going through the smearing routine to compute the combined mass distribution as it should appear. Knowing that the routine models an imperfect detector where some particles escape detection, I used all stable particles, other than neutrinos, neutralinos, and the initial lepton to make this unsmeared calculation. The resulting distribution, shown in Figure 10, is similar to a gaussian, but cut off at the right. The mean was about 2.5 GeV greater than the mean of the data that included the error.

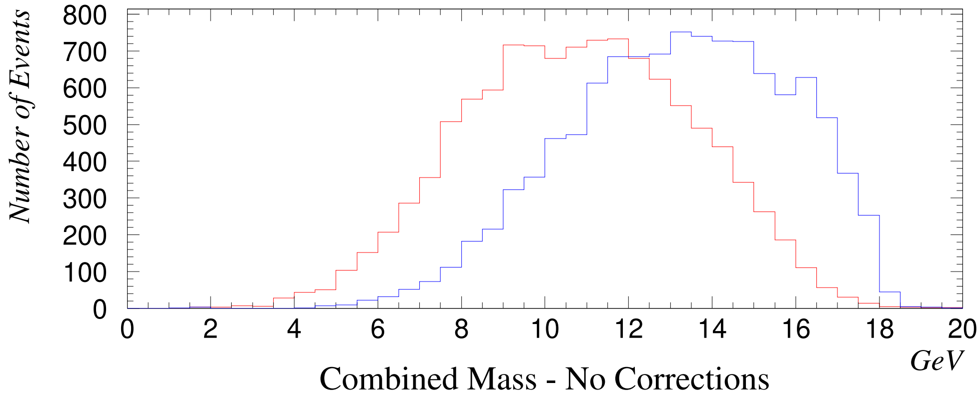

Figure 10: Red - Smeared data (includes error); Blue - Unsmeared data(no error).

6.1 Misidentifications

There were two reasons for this shift. First, the smearing routine assumes that the NLC will not have good particle identification abilities. This means that there are five types of particles that it can distinguish: charged particles that interact in the electromagnetic calorimeter (electrons and positrons), uncharged particles that appear there (photons), charged hadrons (pions, kaons, and protons), uncharged hadrons (kaons and neutrons), and muons. The interaction regions for stable particles are shown in Table 10. Unfortunately, the design for the NLC currently includes no method to distinguish pions from charged kaons and protons, or neutral kaons from neutrons. Since the most commonly formed stable hadrons are neutral kaons and pions, the design will treat all charged kaons and protons as pions, and all neutrons as neutral kaons.

Table 10: Detection of Stable Particles

Particle	$e^\pm$	γ	$\pi^\pm$	$K^\pm$	$p^\pm$	K^0	n^0	$\mu^\pm$	$\widetilde{\chi}_1^0$
Tracking Chamber	$\surd$		$\surd$	$\surd$	$\surd$			$\surd$	
E.M. Calorimeter	$\surd$	$\surd$							
Had. Calorimeter			$\surd$	$\surd$	$\surd$	$\surd$	$\surd$		
Muon Detector								$\surd$	

A possible method to distinguish particles is to compute their mass. This is possible only with a good measurement of momentum and either energy or velocity. For charged particles, there is good momentum measurement, but there is none at all for neutral particles. Furthermore, the hadronic calorimeter is quite imprecise, so the measurement of energy will always be bad. The NLC currently includes no plans for a Cerenkov radiation monitor, which measures the speed of charged particles. Therefore, it is impossible with the current design to measure the masses of hadrons directly.

For neutral particles, the momentum is measured from the energy by assuming the mass to be the mass of the neutral kaon. This calculation yields a momentum that is too high for neutrons, because the mass of the kaon is lower than the mass of the neutron. For charged pions, kaons, and protons, the energy is calculated from the momentum, assuming the particle to be a pion. Since the mass of the pion is small, the energy calculations for the neutron and the kaon come out too low. Thus, the total measured energy is too low while the momentum is too high. This means that the difference in their squares will be small, causing the combined mass measurement to decrease. This effect is significant, but does not account for most of the error, as shown by Figure 11.

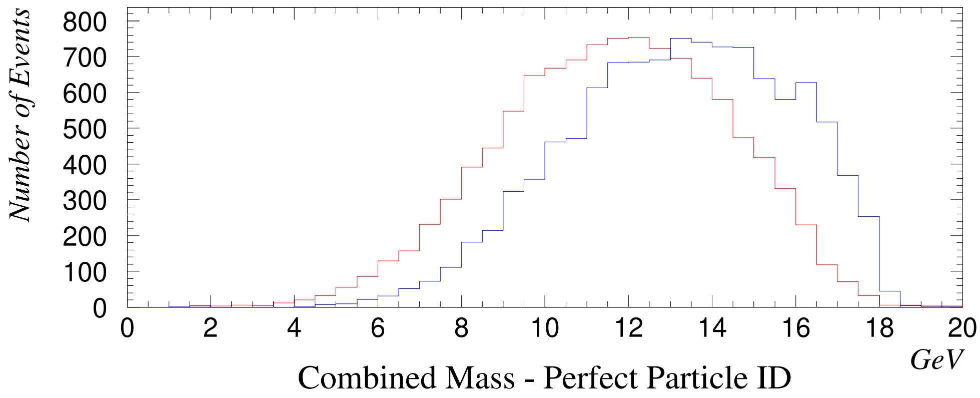

Figure 11: Red - Smeared data; Blue - Unsmeared data. The smeared distribution is slightly better when using the appropriate masses for protons, neutrons, and charged kaons. Thus, misidentification accounts for only a fraction of the error in the combined mass calculation.

6.2 Lost Particles

Losing a particle entirely generally has a much greater effect than simply misidentifying it, as shown by Figure 12. The detector may lose particles for several reasons. They may escape down the beampipe, although it is quite narrow, or they may simply be missed, even when they pass through the detector. This simulation assumes that 2 percent of all particles that pass through the detector escape due to some inefficiency. Another reason that particles escape detection is that they have low momentum. For charged particles, momentum is measured by the radius of the curve that they follow through a magnetic field. For particles with small transverse momentum (momentum perpendicular to the magnetic field), this radius is very small. Thus, some particles may curl up inside the detector, and never reach even the tracking system. With the current detector design, this will happen for all charged particles with transverse momentum less than 240 MeV. Furthermore, all photons with less than 500 MeV will be lost in the noise of the electromagnetic calorimeter.

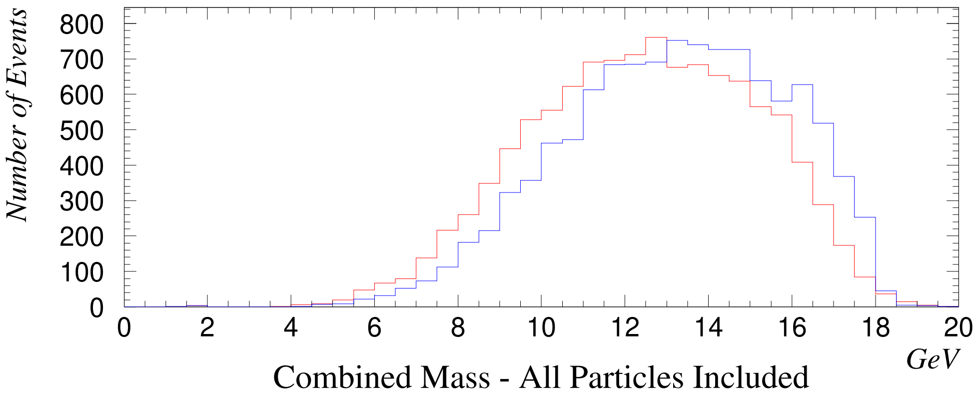

Figure 12: Red - Smeared data; Blue - Unsmeared data. The effect of lost particles is much more important than the effect of misidentifications. The smearing routine has much less effect if all particles are detected.

6.2.1 Charged Particles

The stable charged particles used in this calculation are all either protons or charged kaons or pions. However, most events have very few protons and charged kaons, and these are usually higher momentum, so most are detected. The transverse momentum distribution for these particles is shown in Figure 15. However, many low momentum pions are produced; their most probable transverse momentum is below 240 MeV, also shown in Figure 15. Still, pions account for a small fraction of all the stable particles, and most of them are detected. The effect of losing pions, shown in Figure 13, is even smaller than the effect of particle misidentification. Therefore, the neutral particles must account for most of the effect of missing particles.

6.2.2 Neutral Particles

Four types of stable neutral particles may appear in this decay mode: neutrons, short and long neutral kaons, and photons. Most kaons and neutrons will be detected, as the magnetic field has no effect on neutral particles. The simulation removes only those that escape down the beam pipe, and 2 percent of the rest at random. Because this is so rare, losing neutrons and neutral kaons has almost no effect on the combined mass measurement. This is shown in Figure 16.

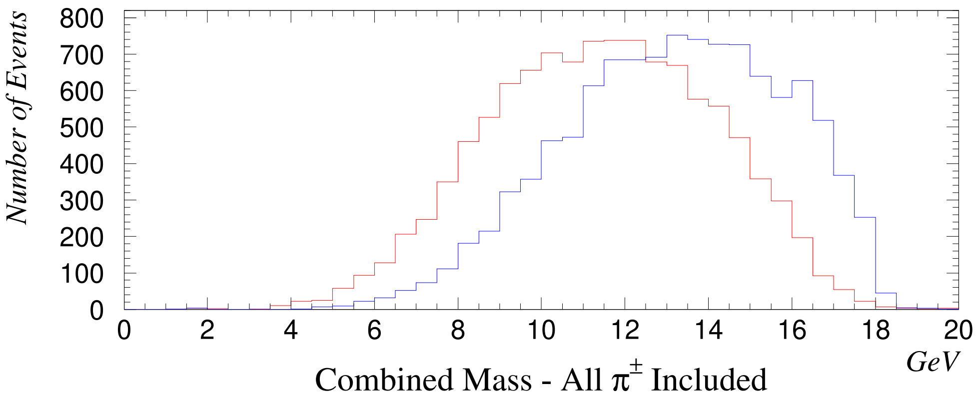

Figure 13: Red - Smeared data; Blue - Unsmeared data (all particles included). The detection of all the pions has a small but significant effect to correct the error in the combined mass measurement

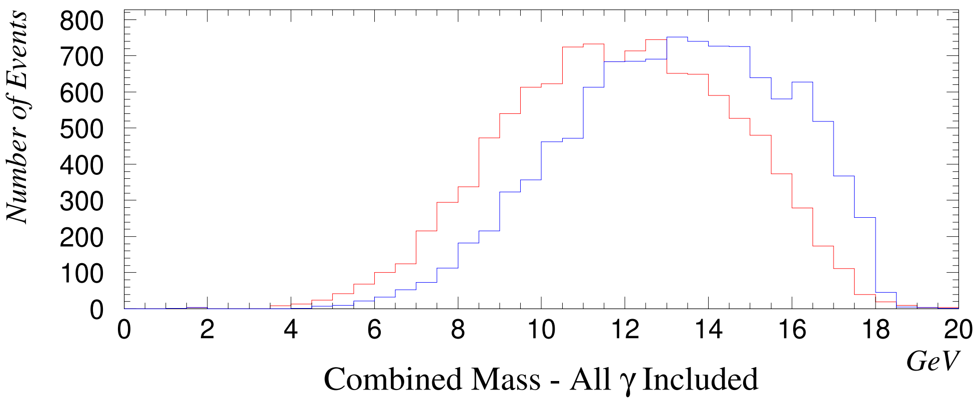

Figure 14: Red - Smeared data; Blue - Unsmeared data (all particles included). Including all photons in the combined mass calculation corrects much of the bias due to smearing.

However, most of the stable particles produced are photons. Many of these have less than 500 MeV of energy, as shown in Figure 15. With the current design it is difficult to distinguish the showers that these produce in the detector from noise. Thus, the loss of photons has an enormous effect on the combined mass calculation, as shown in Figure 14. This is the most important reason for the bias in the combined mass measurement.

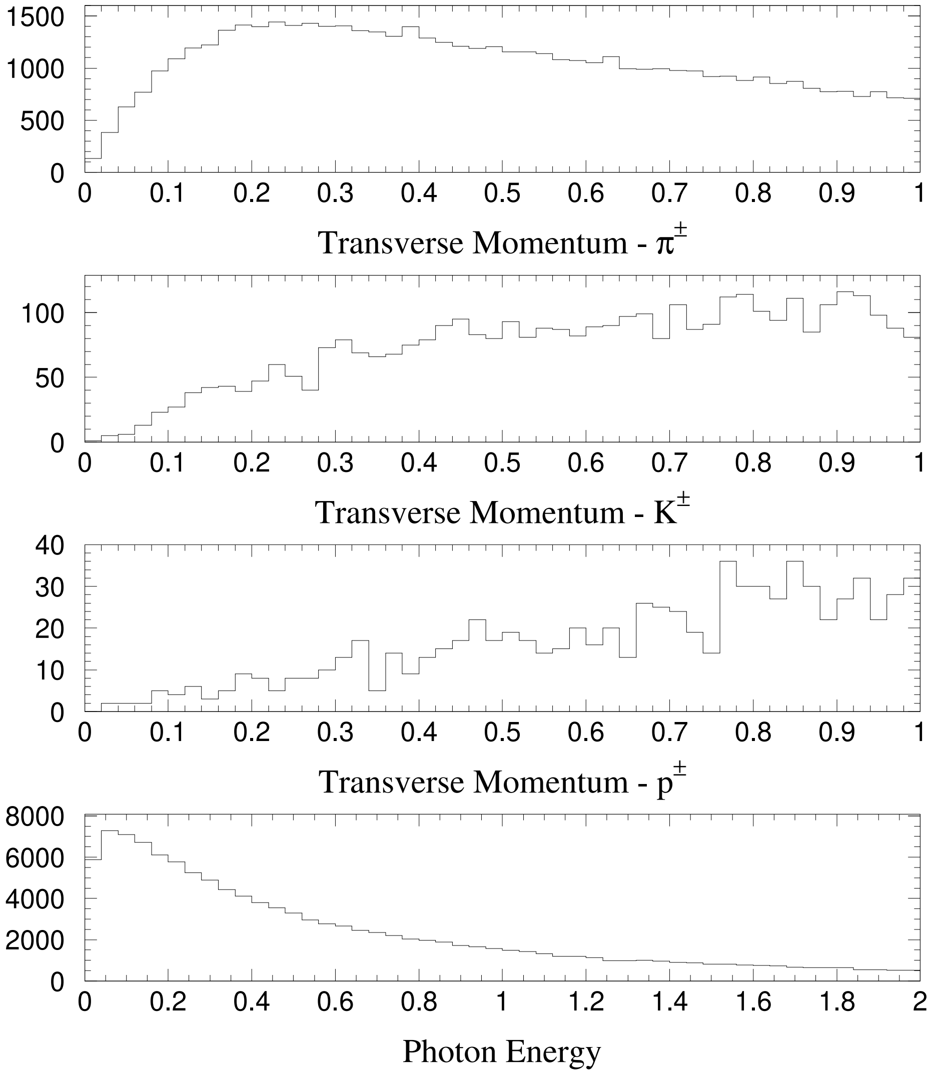

Figure 15: From top: Transverse momentum distributions for $\pi^{\pm}$, $K^{\pm}$, and protons, and energy distribution for photons. For kaons and protons, there are quite few events lost because of small transverse momentum (below 240 MeV); many more pions are lost this way. Very many photons are lost to noise below 500 MeV.

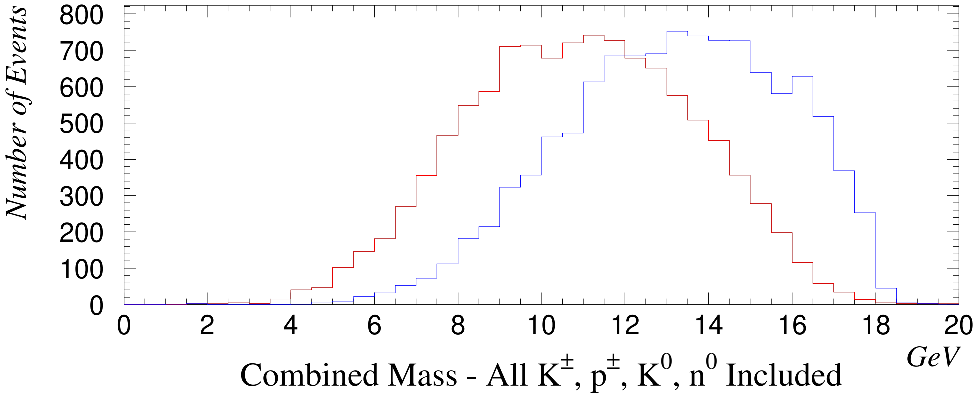

Figure 16: Red - Smeared data; Blue - Unsmeared data (all particles included). Including all protons, neutrons, and kaons (charged or uncharged) has very little effect on the mass calculation, since so few are produced, and so few of those produced are lost. Thus the only lost particles important in this study are photons and pions.

6.3 Results

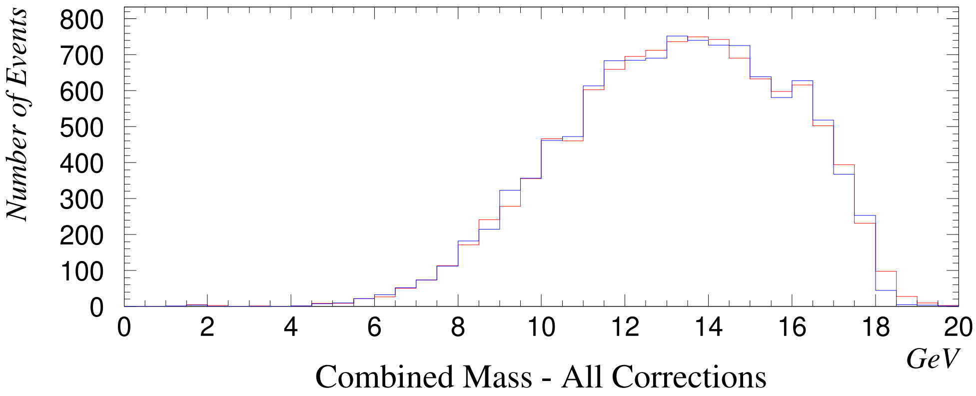

Figure 17: Red - Smeared Data; Blue - Unsmeared Data. This plot shows the mass distribution using the appropriate masses for neutrons, protons, and charged kaons; and including all stable particles in the calculation.

The reasons stated above can account for all of the bias in the combined mass calculation. Including both effects in the calculation results in nearly perfect agreement between the smeared and unsmeared data. This agreement is shown in Figure 17.

7 Conclusions

At this point in the study, it is not possible to determine what should be done to improve the design of the NLC detector. While better sensitivity to photons will decrease the bias in the combined mass calculation, this is only part of a solution. There are many small factors that hurt the combined mass calculation, and thus the calculation of the supersymmetric masses. It may be feasible to begin tracking closer to the beam, in order to detect more charged tracks, or to improve particle identification. This can be done by incorporating a Cerenkov radiation detector, which measures the speeds of particles, or to improve the hadronic calorometry. However, each improvement will likely have only a small effect. Thus, it is important to study how each source of error contributes to the discrepancy in the sparticle mass measurement.

8 Further Studies

There are two areas in Point 4 chargino production that require further study. First, a study of improvements to the detector is necessary. Without this, it will be impossible to properly analyze charginos that hadronize. It is then necessary to incorporate Standard Model background into the data set. This might produce damaging overlaps, especially since the cross section for STMD events is so high.

References

[1] Nick Danielson. *Determining the Mass of the Sneutrino and the Chargino By Examining the Sneutrino Sneutrino Production Mode.* COLO HEP 404, 1998.

[2] Elizabeth Goodman. *The Search for the Supersymmetric Selectron.* COLO HEP 398, 1997.

[3] David Wagner. *NLC SUSY Generation and Analysis, ver. 1.1.* 1998.

[4] Brook Williams. *Study of the Production of SuperSymmetric Particles.* COLO HEP 402, 1998.